ENGINEERING

A machine-learning–powered spectral-dominant multimodal soft wearable system for long-term and early-stage diagnosis of plant stresses

Qin Jiang[1]†, Xin Zhao[1]†, Tiyong Zhao[1]†, Wenlong Li[2,3]†, Jie Ye[4]†, Xingxing Dong[1], Xinyi Wang[4], Qingyu Liu[4], Han Ding[1], Zhibiao Ye[4], Xiaodong Chen[3]*, Zhigang Wu[1]*

Addressing the global malnutrition crisis requires precise and timely diagnostics of plant stresses to enhance the quality and yield of nutrient-rich crops, such as tomatoes. Soft wearable sensors offer a promising approach by continuously monitoring plant physiology. However, challenges remain in identifying direct physiological indicators of plant stresses, hindering the development of accurate diagnostic models for predicting symptom progression. Here, we introduce a machine-learning-powered spectral-dominant multimodal soft wearable system (MapS-Wear) for precise, long-term, and early-stage diagnosis of stresses in tomatoes. MapS-Wear continuously tracks leaf surrounding temperature, humidity, and unique in-situ transmission spectra, which are critical stress-related indicators. The machine learning framework processes these multimodal data to predict gradual stress progression and diagnose nutrient deficiencies in plants over 10 days earlier than conventional computer vision methods. Moreover, MapS-Wears enables portable and large-scale screening of grafted tomato varieties in greenhouses, accelerating the identification of compatible grafting combinations. This demonstration highlights the potential for high-throughput plant phenotyping and yield improvement.

INTRODUCTION

Affected by various conflicts, climate change, and the global pandemic, nearly 2.8 billion people worldwide cannot afford a healthy diet, which leads to malnutrition (*1*). In consequence, imbalanced nutritional intake often results in undernutrition (*2*), obesity (*3*), and other diet-related diseases (*4*), imposing a notable burden on the economies and societies. As a naturally nutritious food rich in vitamins, proteins, and dietary fibers (*5*), tomatoes are among the most widely produced agricultural products (*6*). However, high-quality tomato production faces substantial challenges due to various imperceptible biotic stresses [e.g., diseases (*7*) and pests (*8*)] and abiotic stresses [e.g., unsuitable temperature (*9*), drought (*10*), and nutrient deficiencies (*11*)], which are often difficult to detect early. For example, red spider mites are among the most destructive and hard-to-control pests for tomatoes, causing host plants to whiten and die within weeks without prompt pesticide treatment (*12*). Moreover, deficiencies in essential nutrients—such as nitrogen (N), phosphorus (P), and potassium (K)—can severely hinder plant growth and fruit production (*13*). Therefore, advanced techniques for the precise and timely diagnosis of plant stresses are critical for proactive plant management, reducing costs, and improving production efficiency. Noting that tomatoes are often considered as a model plant, this technique can potentially be extended to other crops as well.

As a crucial organ of plants, leaves not only support vital physiological processes (*14*)—such as transpiration, photosynthesis, and nutrient transport—to maintain plant health but also serve as primary indicators of plant stresses. Thus, various conventional technologies have been proposed to detect leaves' physiological information for diagnosing plant stresses, including biomolecular analysis (*15*, *16*), portable sensors (*17*–*19*), volatile organic compound (VOC) profiling (*20*), computer vision (CV) (*21*), and spectroscopy (*22*, *23*). Biomolecular analysis provides precise plant stress diagnosis by detecting molecular changes, yet it requires destructive tissue sampling and disrupts natural plant growth. Portable sensors (such as optical, moisture, and impedance sensors) enable convenient real-time and on-site stress diagnosis, while their rigid and bulky mechanism can damage plants. VOC profiling provides nondestructive diagnosis methods by analyzing VOCs emitted by plants but is highly susceptible to environmental factors like temperature and wind. Among these, CV and spectroscopic methods are widely used due to their advantages of real-time, noninvasive, and convenient monitoring. Using trichromatic (*24*) and thermal (*25*) cameras to capture leaf images, CV methods can recognize symptoms associated with plant stresses, having become one of the mainstream noninvasive methods for plant health monitoring (*26*, *27*). However, its recognition accuracy can be compromised by environmental factors such as object obstruction, light fluctuations, and dust contamination. Spectroscopic methods offer a promising approach to addressing these challenges by analyzing spectral signatures of leaf pigments—such as chlorophylls, anthocyanins, and carotenes—which serve as essential biomarkers for plant stresses (*28*, *29*). Nevertheless, bulk spectroscopic systems require mechanical fixation to maintain the leaf at the focal position, severely limiting their ability to continuously and effectively track plant health and stresses for the long term.

Recently, soft wearable sensors, known for their unique deformability and biocompatibility, have been introduced for plant health monitoring. These sensors can be directly attached to leaves to continuously collect diverse physiological information [e.g., water content

[1]State Key Laboratory of Intelligent Manufacturing Equipment and Technology, School of Mechanical Science and Engineering, Huazhong University of Science and Technology, Wuhan 430074, China. [2]Institute of Materials Research and Engineering (IMRE), Agency for Science, Technology and Research (A*STAR), 2 Fusionopolis Way, Innovis #08-03, 138634 Singapore, Singapore. [3]Innovative Center for Flexible Devices (iFleX), Max Planck – NTU Joint Lab for Artificial Senses, School of Materials Science and Engineering, Nanyang Technological University, 50 Nanyang Avenue, 639798 Singapore, Singapore. [4]National Key Laboratory for Germplasm Innovation & Utilization of Horticultural Crops, College of Horticulture and Forestry Sciences, Huazhong Agricultural University, Wuhan 430074, China.
*Corresponding author. Email: chenxd@ntu.edu.sg (X.C.); zgwu@hust.edu.cn (Z.W.)
†These authors contributed equally to this work.

(*30*, *31*), VOC emissions (*32*, *33*), chlorophyll content (*34*), deformation (*35*, *36*), and bioimpedance (*37*–*40*)], and living microclimates (e.g., temperature, humidity, and light intensity) (*41*). However, despite notable advances in these soft sensors, a key challenge remains in establishing quantitative relationships between sensing information and plant stresses. This challenge primarily arises from the limited quality of sensor data and insufficient data analysis capabilities. Although spectroscopic data provides valuable insights into plant health, on-plant wearable sensors that can in situ and continuously track plant spectral variations remain unexplored. Moreover, integrating multimodal data from various complementary sensor types to effectively decouple the influences of multiple stresses has not been fully exploited. These limitations hinder precise and early diagnosis of plant stresses, delaying timely disease treatment and management.

Here, we presented a machine-learning (ML)–powered spectral-dominant multimodal soft wearable system (MapS-Wear) for precise, long-term, and early-stage diagnosis of plant stresses (Fig. 1A and movie S1). MapS-Wear integrates in situ spectroscopic detection with temperature and humidity (T&H) measurements using a soft sensor patch, which can be conformally attached to the abaxial leaf surface. The multimodal data streams from the sensor patch are processed using a custom ML framework, enabling the precise diagnosis of various abiotic and biotic stresses with a high prediction accuracy of 99.2%. Multiple MapS-Wears can be deployed across different plant branches, forming a multisensor network for convenient and precise health status monitoring. Notably, MapS-Wear can detect nutrient-deficient stress in plants over 10 days earlier than the conventional CV method before visible symptoms appear (Fig. 1B). This early diagnosis provides a sufficient window for timely nutrient replenishment targeting health recovery. Furthermore, MapS-Wear can be practically applied for large-scale evaluation of health status across various grafted tomato varieties in greenhouses, assisting researchers in identifying compatible graft combinations to enhance crop quality and yield (Fig. 1C).

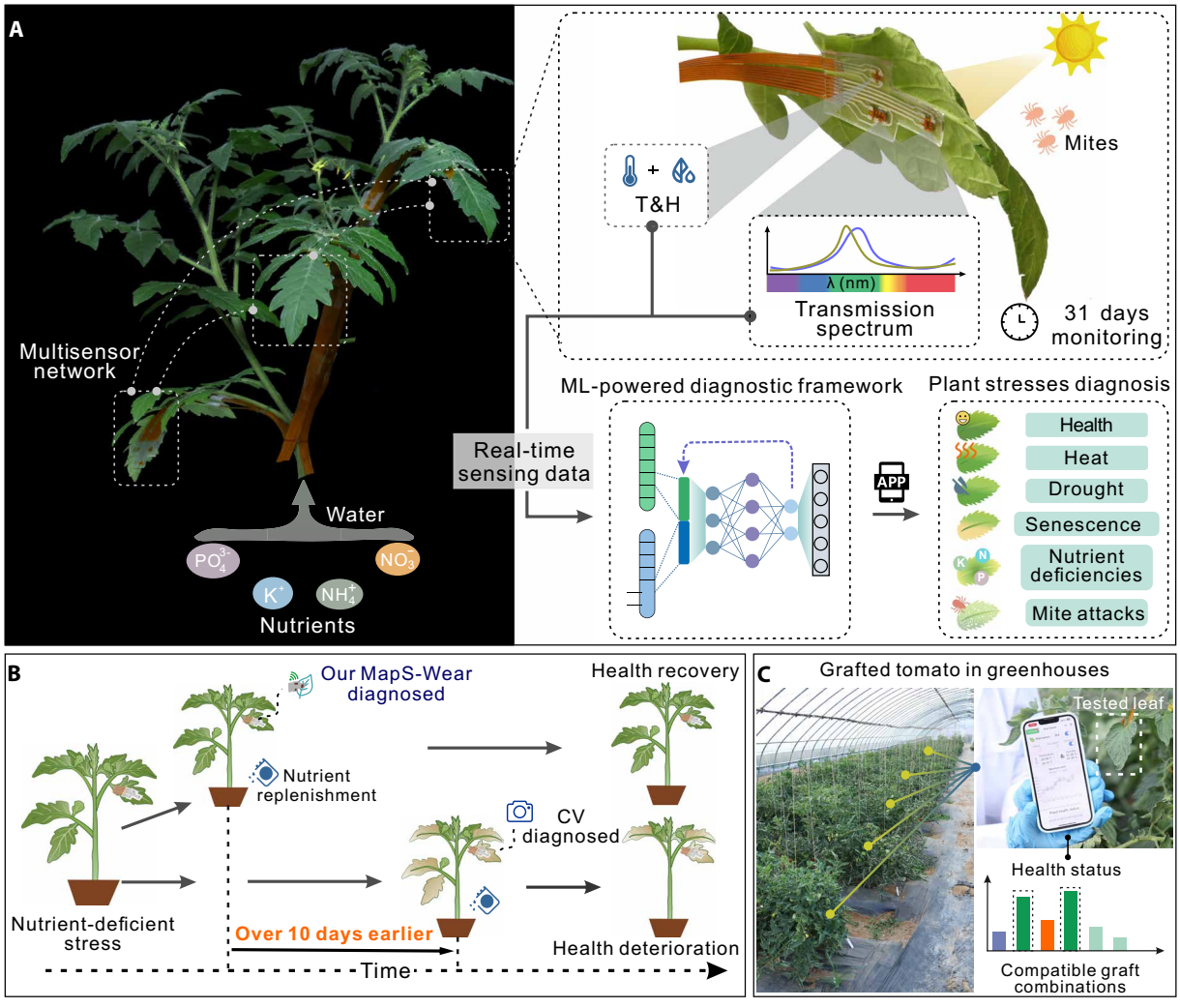

Fig. 1. MapS-Wear for long-term and in-situ diagnosing plant stresses. (**A**) Illustration and photos of attaching the MapS-Wear to live tomato leaves for real-time plant stress diagnosis. (**B**) Illustration showing the MapS-Wear's ability to diagnose nutrient deficiency symptoms at an early stage (10 days earlier than CV diagnosis), with prompts for timely nutrient replenishment to aid plant health recovery. (**C**) Practical application of the MapS-Wear for diagnosing the health status of grafted tomatoes and evaluating compatible graft combinations in greenhouses. Photo credit: Q.J., HUST.

RESULTS

Soft sensor patch for the MapS-Wear

The soft sensor patch is a key part of the MapS-Wear for monitoring leaf physiological information (Fig. 2A). It includes two spectral sensors and a T&H sensor assembled on soft and stretchable polydimethylsiloxane (PDMS) substrate, forming a sandwiched structure (fig. S1). To mitigate stress concentrations at the sensor sites during deformation (*42*, *43*), sensors are encapsulated in modulus-gradient PDMS (MG-PDMS) (fig. S2). Liquid metal (LM) traces, with reliable conductivity even under 110% strain conditions, are printed on the substrate to connect sensors and external flat flexible cable for data transmission. Coated with an optimal adhesion layer, the soft sensor patch can conformally attach to the lower epidermis of the leaf, enabling the long-term and reusable collection of transmission spectra and surface T&H data (figs. S3 and S4, and movie S2).

When tomatoes suffer from nutrient deficiencies (N, K, and P) and mite attacks, the content and distribution of pigments in their leaves (chlorophyll, anthocyanins, and carotenoids) are affected (*44*), subsequently leading to visible symptom changes. As each pigment has a specific absorption spectrum, spectroscopic detection methods are widely used to analyze variations in leaves' spectral features for diagnosing plant stresses (*45*–*47*). Unlike the commonly used complex and rigid spectral probes to record large amounts of dense spectral data, we opted for miniature spectral sensor components that can directly contact the leaf surface to capture its transmission spectrum in the visible region (415 to 680 nm) via eight channels.

While raw transmission signals are easily influenced by external lighting variations, spectral transmittance is inherently linked to the intrinsic spectral properties of leaf pigments, providing a more stable measurement. Therefore, we applied the soft sensor patch to leaves with five different health statuses (healthy; N, P, and K deficient; and mite-attacked) to collect their spectral transmittance data (Fig. 2B). Each stress type causes distinct color changes in the leaves, which are related to variations in pigment content (Fig. 2C). Healthy leaves obtain the highest spectral peak at 550 nm (green band), corresponding to their high chlorophyll content. In contrast, N-deficient leaves appear yellow due to hindered chlorophyll synthesis, causing a shift in their spectral peak to 590 nm (yellow band). P-deficient leaves show a purple hue due to anthocyanin accumulation, which results in a high transmittance value at 680 nm (red band). Mite-attacked leaves develop whitish speckles and exhibit reduced pigment contents, as mites extract sap from the leaf mesophyll (*48*), resulting in a lower peak value at 550 nm compared to healthy leaves. Notably, K-deficient leaves show yellowing at the edges while retaining green near the veins, reflecting the spatial variation of chlorophyll levels across the leaf. To assess spatial distribution differences of these pigments, two spectral sensors were designed to separately collect the spectral data from the center and edges of leaves (fig. S5). Therefore, the spectra for K-deficient leaves collected by two spectral sensors exhibit notable differences, especially at 550 nm. The transmittance spectra collected by our soft sensor are generally consistent with those obtained from a benchmark spectrophotometer, validating the sampling accuracy of our sensors (fig. S6). Therefore, the processed spectral transmittance data from leaves with different health statuses show notable differences, highlighting the potential to classify these stresses based on their spectral information.

Apart from spectra sensors, we also incorporate a T&H sensor offering complementary information to improve diagnosis quality by providing physiological insights into plant transpiration. During transpiration, stomata open to release water vapor, causing a microenvironment of lower temperature and higher humidity near the leaf adaxial surface and thus further affecting the physiological process of leaves (*49*). The leaf's transpiration rate (*Tr*) is markedly influenced by stomata status and closely linked to plant health (Fig. 2D). Under drought stress, stomata are close to minimizing water loss, leading to a reduced *Tr*. Senescent leaves also exhibit decreased *Tr* due to decreased stomatal density (fig. S7). To continuously track plant *Tr*, we attached the T&H sensor to the backside of the leaf epidermis, ensuring a gap between the sensor and the leaf epidermis to prevent water vapor accumulation (fig. S8). The T&H information of the leaf and ambient environment was continuously monitored outdoors for 24 hours (Fig. 2E). The T&H value of the leaf and ambient environment remained similar at night, while notable differences were observed due to leaf transpiration during the day. Usually, the humidity difference (ΔH) between the leaf and ambient environment reached its maximum value at midday. Throughout a day of continuous recording, the rigid chamber of a commercial transpiration meter caused damage to the tested leaf, whereas our soft sensor showed no observable effects on the leaf (fig. S9).

To further investigate the daily maximum humidity difference (ΔH_{max}) in response to plant drought and senescence stress, we used the T&H sensor to continuously record data for the long term. We subjected a tomato plant to cyclic drought conditions for 10 days (Fig. 2F and fig. S10). As the soil water content (SWC) gradually decreased from saturation to below 15%, the plant experienced drought stress, causing its branches to wilt. Despite this, the soft sensor remained conformally attached to the leaf, indicating its strong adhesion characteristics (fig. S11). With the decrease of SWC, both ΔH_{max} and *Tr* decreased to low levels. After rewatering, ΔH_{max} and *Tr* increased to high values, and the plant morphology recovered to its normal state. We also tracked the variations in ΔH_{max} as the plant underwent senescence over 21 days (Fig. 2G and fig. S12). During this period, the leaf gradually turned yellow due to cell apoptosis and pigment degradation, leading to a decrease in both ΔH_{max} and *Tr*. Unlike drought stress, the decrease in ΔH_{max} during leaf senescence cannot recover to its normal state. According to these results, the ΔH_{max} and the *Tr* present high correlations [coefficient of determination (R^2) = 0.91], supporting the theoretical deduction (details in note S1 and fig. S13). Furthermore, the ΔH_{max} can serve as an additional indicator to identify plan drought and senescence statuses when it falls below 10% relative humidity (RH).

ML-powered diagnostic framework

Existing plant health diagnostic methods, such as CV, mainly focus on diagnosing leaves until distinct symptoms appear, failing to predict the gradual progression of stresses (*21*). Moreover, these methods require large datasets for training models, posing challenges for long-term plant cultivation. To address these limitations, we build up an ML-powered diagnostic framework that can continuously diagnose plant stresses with high accuracy while reducing the need for extensive training datasets (Fig. 3A).

The ML-powered diagnostic framework consists of two components: a T&H discriminator (THD) and a spectral diagnostic model (SDM) (note S2 and fig. S14). We observed that leaves under drought and senescent conditions cause disturbances in their spectral transmittance due to changes in leaf thickness and symptoms. These results may lead to misdiagnosis during spectral analysis, while integrating

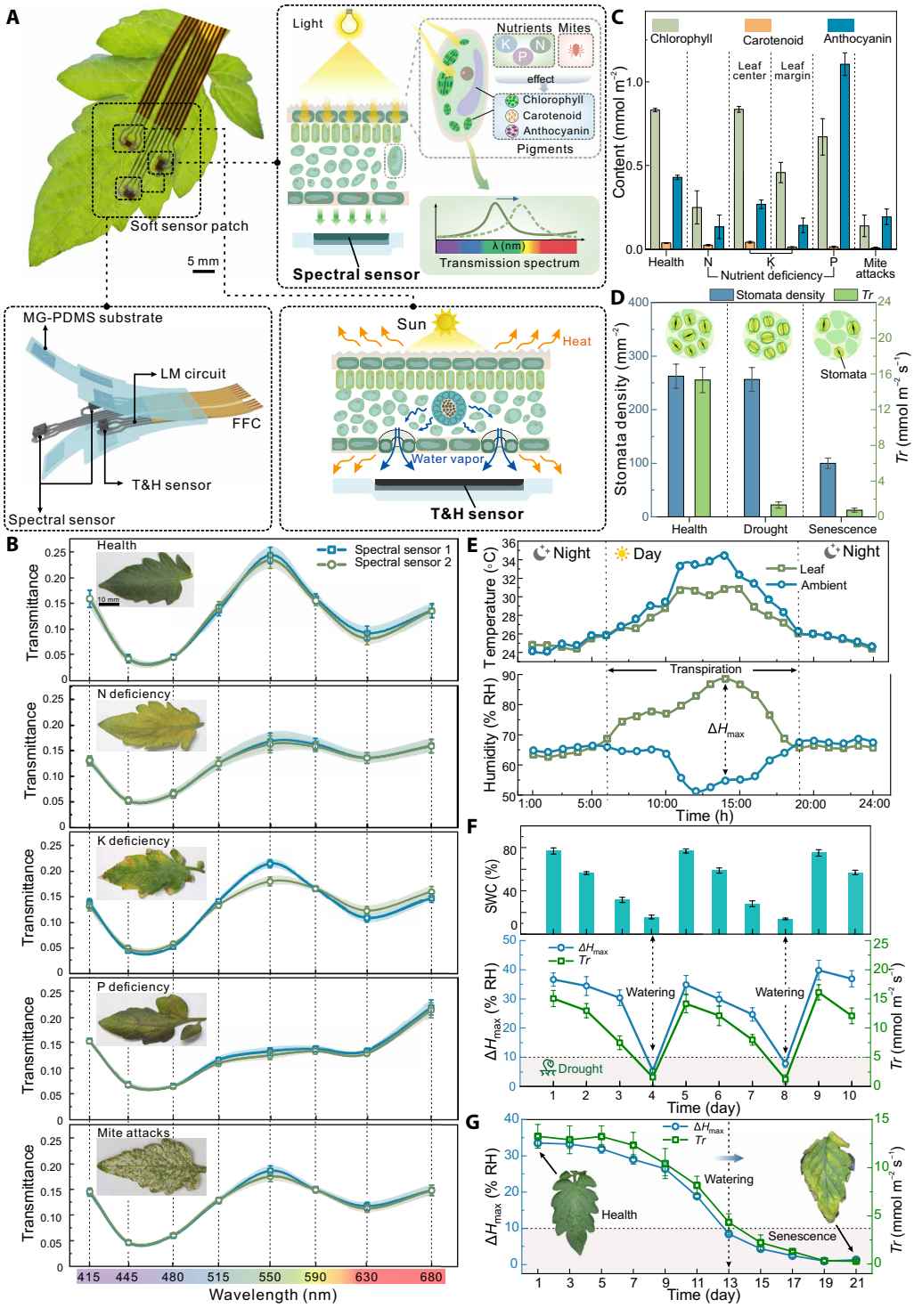

Fig. 2. Working principle and characterization of the soft sensor patch. (**A**) Schematic illustrating the soft sensor patch attached to the abaxial surface of a tomato leaf for detecting T&H and transmission spectral information. Top left: Photo of the soft sensor patch attached to the abaxial leaf surface. Bottom left: Exploded structural view of the soft sensor patch. Schematics of leaf physiological information detection using the spectral sensor (top right) and the T&H sensor (bottom right). (**B**) Spectral transmittance of various leaf statuses, with data collected from 100 leaves per status. SDs are represented by both color shading and error bars. (**C**) Variations in leaf pigment content under different stress conditions. (**D**) Analysis of stomata density and *Tr* among healthy, drought, and senescent leaves. (**E**) Continuous monitoring of ambient and leaf surface T&H fluctuations over 24 hours. RH, relative humidity. Δ*H*, the difference of leaf surface and ambient humidity. (**F**) Response of ΔH_{max} and *Tr* to SWC changes over a 10-day drought cycle. (**G**) Variations in ΔH_{max} and *Tr* of a leaf undergoing gradual senescence over 21 days. Photo credit: Q.J., HUST.

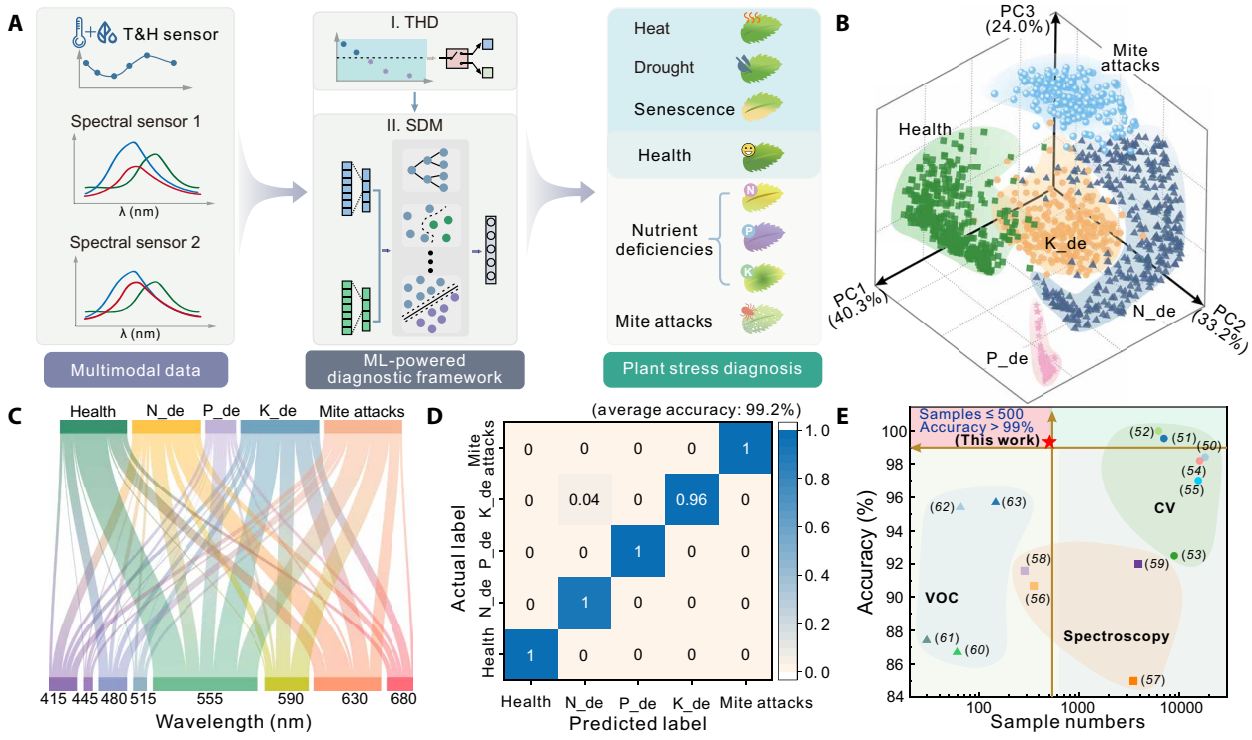

Fig. 3. ML-powered diagnostic framework for multiple plant stress diagnosis. (**A**) Schematics of plant stress diagnostic process. (**B**) 3D visualization of kPCA differentiating various plant stresses based on processed spectral transmittance data. The explained variance ratios are labeled for each PC. N_de, N deficiency; K_de, K deficiency; P_de, P deficiency. (**C**) Sankey diagram depicting the relative contribution of different wavelengths to plant stress classification. (**D**) Confusion matrix demonstrating the recognition accuracy of various plant stresses, with an average accuracy of 99.2%. (**E**) Comparative results highlight our approach's performance in sample size and diagnostic accuracy compared to other related studies, with reference numbers labeled. THD, T&H discriminator; SDM, spectral diagnostic model.

T&H data helps mitigate such an issue (fig. S15). For example, THD can help correct potential misdiagnoses when SDM and CV methods are both influenced by leaf senescence stress (fig. S16). Given their distinct strengths, we integrated THD and SDM to fully exploit their complementary diagnostic capabilities. The THD first differentiates heat, drought, and senescence stress, filtering out possible disturbances to the transmission spectral data. After excluding these confounding factors, SDM is then used to precisely identify nutrient deficiencies (N, K, and P) and mite attacks (movie S3).

After data processing, the processed spectral transmittance corresponding to various leaf health statuses can be clearly distinguished using kernel principal component analysis (kPCA) (Fig. 3B and fig. S17). The three-dimensional (3D) cluster results show that different stress classes are well-separated, with three principal components (PC1, PC2, and PC3) accounting for 97.5% of the total explained variance. Therefore, the kPCA results indicate effective data cleaning, ensuring high-quality input for subsequent ML model training. To maximize the extraction of spectral information properties, we implemented an ensemble learning strategy. Moreover, time-series spectral data, collected as the gradual development of unhealthy symptoms in leaves, was incorporated into the model training process to enhance the generalization performance of the SDM (fig. S18). Thus, this approach enables SDM to output the probability of stress progression in plants by analyzing subtle shifts in spectral data over time (note S3 and fig. S19).

To evaluate the contribution of spectral information during the diagnosis, we assessed the feature importance of each wavelength using Shapley additive explanation (SHAP), as shown in Fig. 3C. The SHAP analysis reveals that 555, 590, and 680 nm wavelengths strongly influence stress classifications. The result suggests that the changes in stress symptoms are predominantly reflected in the color variations associated with these specific wavelengths, consistent with the previous spectral analysis of nutrient deficiencies and mite attacks. The output confusion matrix demonstrated that the SDM achieved the highest classification accuracy of 99.2%, outperforming other typical models (Fig. 3D and fig. S20). Compared to other related works on tomato plant stress diagnosis in terms of sample size and accuracy (*50*–*63*), our work offers a unique advantage by achieving high diagnostic accuracy of more than 99% with a small training dataset of fewer than 500 leaves (Fig. 3E and table S1). As discussed in the previous section, such a high efficacy can be attributed to the in situ spectral detection, which provides high-quality and direct stress-related features, thereby reducing large training dataset requirements and enhancing model performance.

Briefly, our ML-powered diagnostic framework well exploits complementary multimodal information from the T&H and spectral sensors, offering a convenient and highly precise platform to diagnose various plant stresses. Specifically, THD is effective in identifying thermal and moisture-related stresses (e.g., heat, drought, and senescence), while SDM excels in detecting nutrient deficiencies and mite attacks. By integrating THD and SDM, the diagnostic framework provides a more comprehensive and accurate assessment of plant stresses. Moreover, the framework demonstrates stable diagnosis under various disturbances (e.g., wind exposure, water

spray, and heat conditions), simulating commonly seen outdoor environments (fig. S21).

MapS-Wear in plant stresses diagnosis and further extension

Having demonstrated the ability of our MapS-Wear for in situ, long-term, and convenient diagnosis of plant stresses, we applied the system to establish a sensing network, enable early-stage diagnosis of nutrient deficiencies, and conduct high-throughput screening of grafted tomatoes in greenhouses. These demonstrations exhibit MapS-Wear's potential from laboratory validation to practical agricultural implementation.

We deployed a sensing network on an individual plant to investigate how different plant parts respond differently to stresses, such as N-deficient stress in this study. By attaching three soft sensor patches to various branches of a tomato plant (from lower to upper leaves), we established a multisensor network to monitor the plant's health status over 31 days (Fig. 4A). The soft sensor patches can be customized to appropriate sizes, facilitating adaptive attachment to various leaf shapes (fig. S22). To induce N-deficient stress, we cultivated the plant in an N-deficient solution. The probabilities of N deficiency for each leaf, denoted as *P(N)*, were output by MapS-Wear (Fig. 4B). On the 13th day, the *P(N)* for the lower leaf first reached the diagnostic threshold, where it had the highest value among all classifiers, confirming the diagnosis of N-deficient stress. As the plant continued to endure N-deficient stress, the *P(N)* values for both the lower and middle leaves progressively increased, corresponding to increasingly obvious visual symptoms (sequential photos in fig. S23). On the 21st day, the *P(N)* for the lower leaf exceeded 60%, accompanied by distinct yellowing symptoms. To prevent further deterioration of leaves, we replenished the N nutrient in the tomato plant. However, the lower and middle leaves showed irreversible yellowing to senescence, as diagnosed by MapS-Wear (fig. S24). In contrast, the upper leaf remained healthy after N supplementation. During the long-term experiment, we also recorded these test leaves' length variation to investigate the soft sensor patch's impact on natural growth (fig. S25). The results show that the lower leaf and its side leaves maintained stable length, indicating that these leaves were already matured. In contrast, the middle and upper leaves exhibited gradual length increases as they continued growing, with their side leaves showing similar growth rates. These findings indicate that our soft sensor patch remains stable and has negligible on leaves' natural growth. Moreover, plant height variation was recorded, revealing a slowed growth rate under the N-deficient condition and rapid recovery after N supplementation (fig. S26). By establishing a comprehensive sensing network for convenient and simultaneous monitoring of plant health, this study revealed that the lower leaves are more sensitive to N-deficient stress, consistent with plant physiology (*44*). Moreover, this finding can be extended to other nutrient deficiencies (K and P), suggesting that MapS-Wear attached to the lower leaves would enhance its diagnostic sensitivity.

Furthermore, we demonstrate MapS-Wear's capability for early-stage diagnosis and provide efficient windows for the timely treatment of nutrient deficiencies. Soft sensor patches were attached to three leaves on the second-from-bottom branch of each plant to monitor their health status under K-deficient stress (Fig. 4C and fig. S27). After these plants experienced K-deficient stress, the probabilities of K deficiency for each leaf, denoted as *P(K)*, were diagnosed by MapS-Wear (fig. S28). The CV method was also applied to monitor the health variation of these leaves for comparison. During the experiment, a dynamic diagnostic threshold—where *P(K)* peaked relative to other classifiers—was used to determine K-deficient stress. For Leaf l, our system successfully diagnosed its K-deficient stress on the 11th day. Subsequently, we immediately replenished the K nutrient to prevent further leaf deterioration. Because of the K replenishment at an early stage, Leaf 1 gradually recovered to a healthy status (photos in fig. S29A). In contrast, the CV method failed to detect subtle symptom changes in Leaf 1 throughout the entire experiment (fig. S30). For Leaves 2 and 3, we delayed the K replenishment until the *P(K)* exceeded 60 and 90%, respectively. Notably, MapS-Wear provided an earlier diagnosis by more than 10 days compared to the CV method, highlighting the superior performance of our spectral-based detection approach over the conventional vision-based method. Despite the subsequent K supplementation, these two leaves underwent irreversible deterioration, ultimately exhibiting severe K deficiency symptoms and eventually turning senescent, which was diagnosed by MapS-Wear (figs. S28 and S29, B and C). Consequently, the *P(K)* values for Leaves 2 and 3 presented inaccuracies that were influenced by their senescent states. After the 31-day experiment, these three plants exhibited different growth phenotypes. For instance, the plant with Leaf 1 grew lushly because of the timely treatment of K deficiency, whereas plants with Leaves 2 and 3 showed sparse leaves due to the delayed K replenishment (photos in fig. S29D). Therefore, MapS-Wear provides researchers with a sufficient time window for early-stage diagnosis and thus to make an active intervention, such as timely nutrient-deficiency treatment, which helps plants to recover to a healthy status.

Last, we further extended MapS-Wear to practical agriculture settings, in greenhouses, for large-scale evaluation of the compatibility of grafted tomatoes. Tomato grafting is widely applied in agriculture to enhance disease resistance (*64*), improve stress tolerance (*65*), and boost crop yields (*66*). In grafted tomatoes, nutrients are transferred from the rootstock to the scion through water transport (Fig. 4D). However, graft incompatibility limits nutrient transport, resulting in nutrient deficiencies in these plants (*67*). Hence, diagnosing the health status of these grafted tomatoes can guide evaluating the compatibility of various grafting combinations. Based on this, we deployed MapS-Wear in greenhouses for on-site diagnosis of tomato graft compatibility (Fig. 4E and movie S4). Compared to commercial sap analyzer to measure plant nutrient contents, our system offers a noninvasive, portable, and real-time diagnostic approach that reduces the operation time from hours to seconds (Fig. 4F). In this study, a single type of tomato scion grafted onto different varieties of rootstocks to form 50 types of graft combinations. Using MapS-Wear, we diagnosed the health status of these grafted tomatoes to assess their graft compatibility (Fig. 4G). The growth status of different graft combinations was mapped, offering researchers valuable insights to identify compatible combinations within healthy graft groups (Fig. 4H). Nutrient contents of these tomatoes were also measured through sap analysis, serving as a benchmark for nutritional assessment. Comparing the results from MapS-Wear with those from sap analysis, MapS-Wear achieved a high evaluation accuracy of 88% (more details in Materials and Methods and table S2). The incorrect diagnoses may be attributed to plants experiencing other stresses not included in our current datasets but exhibiting similar symptoms, suggesting that further optimization is necessary in the future. Nevertheless,

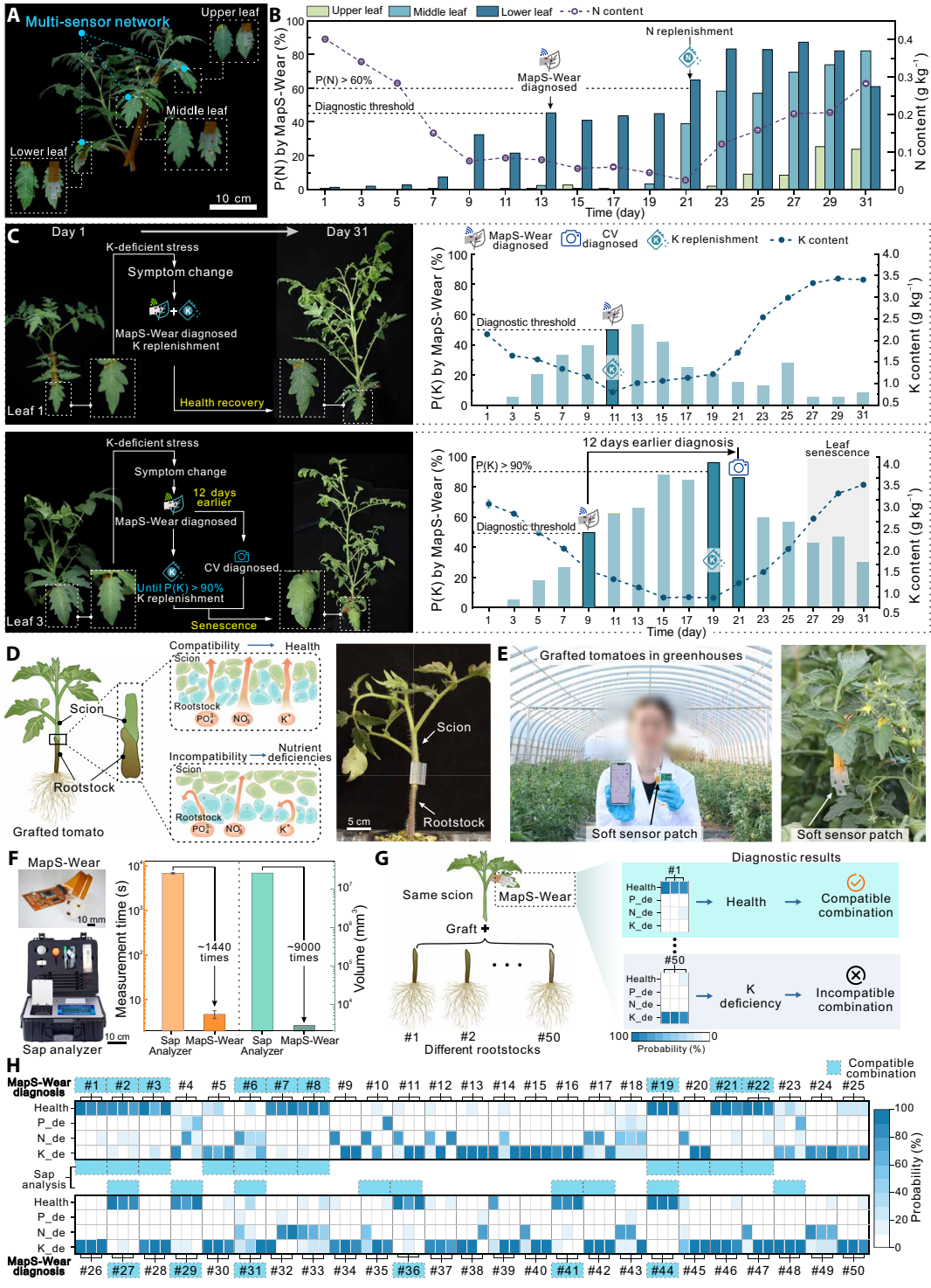

Fig. 4. Demonstrations of live plant stress diagnosis and graft compatibility evaluation using the MapS-Wear. (**A**) Photo showing three soft sensor patches attached to a tomato plant's upper, middle, and lower leaves, forming a multisensor network for stress diagnosis. (**B**) Variation of *P(N)* by MapS-Wear for lower to upper leaves during N-deficient stress and subsequent N replenishment over 31 days, along with overall plant N content measurements. (**C**) Continuous diagnosis of three tomato plants experiencing K-deficient stress and subsequent K replenishment over 31 days. Photos and flow diagrams outline the experiment process, while charts show variations in *P(K)* by MapS-Wear and overall plant K content. (**D**) Schematics and photo of grafted tomato. (**E**) Photos of applying the MapS-Wear for high-throughput screening of grafted tomatoes in greenhouses. (**F**) Comparison between the Maps-wear and commercial sap analyzer regarding measurement time and volume. (**G**) Schematics illustrating the MapS-Wear assessing graft compatibility across different combinations. The same tomato scion was grafted on different rootstock varieties to form 50 combinations. (**H**) Heatmap showing diagnostic probabilities of health status for various grafted tomato groups. The compatible combinations diagnosed by the MapS-Wear and sap analysis are highlighted in blue. Three plants were diagnosed per graft group. Photo credit: Q.J. and X.Z., HUST.

MapS-Wear demonstrates a considerable potential for practical application in agricultural management and production.

DISCUSSION

In this paper, we propose a MapS-Wear that can be conformally attached to the abaxial leaf surface, enabling in situ, long-term, and early-stage diagnosis of plant stresses. The system introduces a unique on-plant spectral detection approach to continuously track the variation of leaf transmission spectra, which can be direct indicators to reflect stresses from nutrient deficiencies and mite attacks. Simultaneously, T&H information of leaves is also recorded to assess plant transpiration, helping to distinguish plant status under heat, drought, and senescence conditions. By well exploiting these multimodal data, an ML-powered diagnostic framework was built to precisely diagnose various abiotic and biotic plant stresses throughout their gradual progression.

Further, our MapS-Wear has been demonstrated for practical tomato stress diagnosis, extending from laboratory validation to agricultural implementation. By incorporating multiple MapS-Wears into a sensing network, the system enables convenient and accurate stress diagnosis across individual plants from the lower to the upper leaves. Compared to existing studies on plant soft wearable sensors (*32*–*35*, *37*, *41*), our MapS-Wear not only achieves the earliest visual-based detection time for plant stresses but also establishes an integrated system for physiology information detection and real-time stress diagnosis (fig. S31 and table S3). The system achieved early diagnosis of nutrient-deficient stress over 10 days earlier than conventional CV methods, allowing a sufficient window for timely intervention to support the plant's healthy recovery. Furthermore, being a convenient and highly precise diagnostic tool, MapS-Wear has been effectively applied for large-scale and high-throughput screening of grafted tomato varieties in greenhouses, assisting researchers in identifying compatible graft combinations to enhance tomato quality and yield. It hints that our approach can be adapted for other plants to enable precise cultivation and intelligent management, offering a potential tool to address the global nutrition crisis.

Future studies will focus on enhancing the reliability and performance of MapS-Wear and expanding its application to other tomato varieties and more plant species. One potential improvement is integrating light-emitting diodes (LEDs) as active incident light sources to minimize interference from ambient light and enable automatic measurement at night. The MG-PDMS substrate could also be replaced with a lighter, softer, and more breathable material (e.g., stretchy gauze or nanofibers) to further reduce the patch's weight and improve breathability. Notably, adapting MapS-Wear for different plant species (e.g., corn, potato, and grape) will require consideration of variations in leaf color, morphology, thickness, and surface texture, which may necessitate adjustments in sensor placement and calibration. For example, differences in leaf thickness affect spectral transmission, necessitating specific spectral calibrations. Expanding the spectral library to include more plant varieties is also necessary to improve the generalization of the ML diagnostic framework. Simultaneously, the ML framework could be further optimized by incorporating advanced algorithms (e.g., large language models) to enhance its data analysis capabilities. Moreover, extending the spectral range (e.g., near-infrared and ultraviolet) may be needed to capture additional physiological information and enhance diagnostic performance. With these modifications, MapS-Wear will further improve its robustness and practical application in agricultural settings.

MATERIALS AND METHODS

Design of the MapS-Wear

The MapS-Wear comprises three subsystems, including a soft sensor patch with T&H and spectral sensors, a data sampling module for collecting and wireless transmitting sensing data and an ML-powered diagnostic framework for diagnosing plant stresses (details of design in fig. S32). The soft sensor patch integrates with a flexible printed circuit board (FPCB)–based data sampling module to form a lightweight (~4 g) plant wearable device (fig. S33). To ensure high stability under large strain, the MapS-Wear incorporates an MG-PDMS structure (fig. S34), with the detailed fabrication process of the soft sensor patch shown in fig. S35. Moreover, the PDMS substrate exhibits excellent optical transparency in visible light (~90% transmittance), high gas permeability (~2000, ~1000, and ~2100 $\mu m^2/s$ for O_2, CO_2, and water vapor, respectively), biocompatible, and low thermal conductivity (~0.27 W/m·K), making it well-suited for fabricating soft sensor patches for plants (*68*). The T&H sensor (SHT41, Sensirion) contains electrical sensing elements for high-precision measurement of temperature (±0.1°C) and RH (±1% RH). The spectral sensor (AS7341, ams-OSRAM) uses photodetectors to convert incident light at specific wavelengths into electrical signals, programmed to use eight channels to capture the visible spectrum (415 to 680 nm). This configuration aims to eliminate interference from near-infrared light, which is abundant in natural sunlight. Both these two sensors can convert physical signals into digital output and communication via the Inter-Integrated Circuit (I^2C) protocol with the bluetooth low-energy microcontroller (NRF52840, Nordic). LM traces, which are biocompatible with plants (*39*, *69*), were printed to connect the sensors for data transmission and fully encapsulated within the PDMS substrate. The hardware circuits are illustrated in fig. S36. The overall hardware cost of the MapS-Wear is approximately $30 for the current proving stage (details in table S4), and it has a high potential for substantial reduction with large-scale production.

Cultivation of tomato plants

Four common tomato varieties were selected as training samples, including red cherry types (Mei Ying 2# and Busan 88) and red salad types (Zhong Shu 4# and China 72–69). These varieties are biologically close relatives and exhibit slight differences in leaf color and morphology, making them suitable for testing and validating the MapS-Wear's diagnostic capabilities across different tomato varieties. These plants were cultivated indoors using hydroponic systems under plant growth lights with 16-hour light and 8-hour dark cycles (fig. S37). Once the plants reached the vegetative growth stage (~30 days after germination), they were subjected to various abiotic and biotic stresses accordingly. To regulate the nutritional state of tomato plants, nutrient solutions were prepared on the basis of Hoagland's formulation, including a full-nutrient solution and solutions deficient in specific nutrients (N, K, and P). Also, some plant groups were subjected to natural infestations by red spider mites (*Tetranychus urticae*).

Details of plant transpiration monitoring

The leaf's transpiration rate was measured using a commercial plant transpiration rate meter (GH1, Heng Mei) by placing the tested leaf

inside the chamber (fig. S9). The meter was programmed to take measurements for 5 min at 1-hour intervals. The soft sensor patch was also attached to the leaf surface to continuously record the leaf and environment T&H information. Meanwhile, the SWC was monitored using a soil moisture probe (SN-3000-TR, PRSENS) inserted into the soil.

Incident light setup for data collection

To ensure stable and consistent spectral data collection in the MapS-Wear system, a uniform white light source (Mi Jia 1S, Xiaomi, 4500 lux, 5000 K color temperature) was used as a controlled illumination source (fig. S38). The incident light was positioned ~30 cm above the tested leaf to maintain consistent light exposure. Moreover, a blackout fabric hood was incorporated to effectively block or reduce external ambient light interference, ensuring reliable spectral measurements. This setup minimizes variations caused by environmental lighting and allows the MapS-Wear system to operate effectively under moderate sunlight conditions (below 15,000 lux) (fig. S39).

Collection of leaf transmission spectral datasets

Leaf samples for ML framework training were collected every 5 days as tomato plants experienced stress. Each collected leaf was placed under the uniform white light provided by a desk lamp (Mijia 1s, Xiaomi; fig. S40). The soft sensor patch was attached to the leaf surface, and its two spectral sensors collected transmission spectra (I_1, I_2) from different locations on the leaf. The ambient incident light (I_{env}) was also captured using an environmental spectral sensor mounted on the FPCB. For each leaf, spectral data from three to five positions of the tested leaf were collected by repeating the above process. Five hundred leaf samples (100 leaves per stress type) in total were gathered to create a comprehensive training dataset that includes 2742 spectral sequences.

The spectral transmittance (T_s) was proposed for further data analysis, which can be defined as,

$$T_{s(i)} = I_i / I_{env}$$

where $i \epsilon [1, 2]$, representing the datasets collected by two spectral sensors. As each spectral sensor covers a broad spectral range from 415 to 680 nm, divided into eight channels, the spectral transmittance sets for different wavelength channels can be expressed as

$$T_{s_x(i),(i=1,2)} = \left[s_{415}, s_{445}, s_{480}, s_{515}, s_{550}, s_{590}, s_{630}, s_{680}\right]$$

where s_x refers to spectral transmittance at wavelength x nm. Then, $T_{s1}$and T_{s2} were normalized as follows

$$\overline{T}_{si,\ (i=1,2)} = \frac{s_{(m)}}{\sum_{t=0}^{8} s_{(t)}}$$

where the $\overline{T}_s$ represents the normalized spectral transmittance and $m \in [415, \ldots, 680]$.

Further data preprocessing included outlier detection and handling using the interquartile range (IQR) method to ensure data consistency. Moreover, kPCA was applied to unsupervised evaluate the impact of data preprocessing on feature quality. By using a kernel function, kPCA projects the data into three PCs, enabling visualization in a 3D feature space and enhancing the separability of nonlinearly distributed clusters. The radial basis function kernel with $\gamma = 0.1$ was used to achieve well-separated clusters. In addition, the explained variance ratios for each PC were calculated to quantify their contribution to cluster separation.

Design of the ML-powered diagnostic framework

The ML-powered diagnostic framework composes the THD and SDM to process multimodal sensor information (details in note S2).

The THD analyzes T&H data to classify leaf status under heat, drought, or senescence conditions using logical thresholds. Heat stress is identified when the ambient or leaf surrounding temperature exceeds 35°C, ensuring timely intervention to prevent adverse effects on tomato growth (*9*). When the ΔH_{max} is lower than 10% RH, the THD initially diagnoses the plant as experiencing drought stress and remind researchers to water the plant. Subsequently, if the ΔH_{max} remains lower than 10% RH; on the following day, the THD diagnoses the tested leaf as undergoing a senescent process.

The training process of the SDM comprises two main phases, including initial training and model optimization (fig. S18), as follows:

1) Initial training. This phase focuses on selecting appropriate base estimators for spectral data classification and establishing pretrained model parameters. We used data from five leaf health categories (health; N, K, P deficiencies; and mite attacks) with distinct symptoms as our pretraining dataset. Then, multiple base estimators were tested on the labeled spectral data, and seven were identified as suitable for further optimization: logistic regression (LR), extra trees (ET), AdaBoost, support vector classifier (SVC), random forest (RF), gradient boost (GB), and decision tree (DT).

2) Model optimization. To enable the model to continuously analyze stress's gradual progression, we augmented the dataset with time-sequenced spectral data reflecting gradual symptom development. With such an enriched dataset, an ensemble learning model was constructed by integrating the above suitable base estimators to enhance its capacity to diagnose plant health status during its gradual changes. A grid search was conducted to optimize the parameters and assign appropriate weights to the base estimators.

Last, THD and SDM were integrated into a unified ML framework deployed on a cloud server (Alibaba cloud, Alibaba) for real-time diagnosis. In practical application, the T&H and spectral data of the leaf and its surrounding environment are transmitted into the ML framework via a network. Then, the ML framework generates classification probabilities and provides an accurate diagnosis of plant health status (details in note S3 and table S5). Compared with other deep-learning methods, the ML framework demonstrates robustness, generalization, and greater suitability for processing tabular spectral data (note S4 and table S6).

As shown in fig. S32, the overall architecture of the MapS-Wear involves three main steps: (i) the data sampling module transmits sensing data to a mobile phone via Bluetooth, (ii) the mobile phone uploads the data to a cloud server, and (iii) the ML framework on the server processes the data and returns the diagnostic result, which is displayed through the mobile phone's WeChat Mini Program interface. Because the sensor data size is very small (~20 bytes), the Bluetooth and network transmission times are nearly negligible. Moreover, the ML-powered diagnostic framework is lightweight and requires minimal computational resources. Therefore, the ML framework processes each sample in ~0.05 ms, enabling MapS-Wear to deliver real-time diagnostics for practical applications.

Long-term nutrient deficiency diagnosis experiments

During the long-term nitrogen (N) and potassium (K) deficiency experiments, the plants were cultivated in an indoor environment to eliminate interference from other stress factors, such as heat, drought, and insect infestations. In addition, photos and sensing data of these tested leaves were recorded daily at 10:00 a.m. To precisely track changes in nutrient content, sap analysis was conducted using a plant nutrient analyzer (YT-TR-ZY, YunTang) by sampling approximately two to three fresh leaves from the middle of the plant every other day (detailed process in fig. S41). After deciding to replenish the deficient nutrient (N or K), the corresponding plant was transferred to a full-nutrient solution.

For the N deficiency experiment (Fig. 4A), red cherry tomatoes (Mei Ying 2#, China Vegetable Seed Technology Co., Ltd) at the flowering stage (60 days after germination) were chosen and cultivated in a hydroponic system. Three soft sensor patches were attached to healthy leaves at different heights of the plant (upper, middle, and lower leaves). The plant was then subjected to an N-deficient solution.

For the K deficiency experiment (Fig. 4D), three red salad tomatoes (Zhong Shu 4#, China Vegetable Seed Technology Co., Ltd) with similar growth statuses (60 days after germination) were selected and cultivated in a hydroponic system. For a controlled setup, three soft sensor patches were separately attached to healthy leaves on the same second-from-the-bottom branch of each plant. Subsequently, these plants were simultaneously placed in a K-deficient solution.

In addition, a ResNet-based CV framework was developed and trained to diagnose plant stresses using images of tested leaves (fig. S42). After optimization, the pretrained ResNet-152–based framework showed the highest prediction accuracy (97.8%) compared to other models (fig. S43).

Graft compatibility diagnosis in greenhouses

The grafted tomato seedlings were prepared by grafting the same scion variety (type: 72-69 tomato, China) onto different tomato rootstock varieties (fig. S44). Particularly, the tomato scion species was included in our training dataset to enhance diagnostic accuracy. Therefore, the tomato leaves remained consistent in type, enabling a systematic and controlled screening of grafting compatibility. Moreover, to prevent the risk of infection, all grafting procedures were conducted in a sterile laboratory environment. The grafted seedlings were then cultivated in greenhouses for 3 months before graft compatibility screening. During this period, any seedlings exhibiting abnormal growth due to infection or severe mechanical damage were excluded from the experiment. Therefore, the tomato seedlings used in the experiment were free from infections or mechanical damage, allowing for a focused analysis of malnutrition caused by grafting incompatibility.

Initially, a small number of grafted tomatoes (26 groups) was randomly sampled to represent the overall health levels of the tomatoes in greenhouses through sap analysis. These grafted tomatoes were categorized into four health levels based on their average nutrient content (N, K, and P) and visible symptoms. Thus, the nutrient content of the third health level served as a benchmark for subsequent experiments (fig. S45).

Subsequently, 50 groups of tomato graft combinations were selected for health status diagnosis (including healthy and N, K, and P deficiencies) and further evaluation of graft compatibility. For each grafted group, three plants were diagnosed using MapS-Wears to comprehensively assess their health status. These plants' health statuses were also evaluated by comparing their actual nutrient content with established threshold benchmarks. Last, comparing diagnostic results from MapS-Wear with sap analysis, compatible grafted plant groups can be identified as healthy (details in table S2).

Spectral properties of leaves

The reflectance and transmittance spectra of leaves in various health statuses (healthy; N, P, and K deficient; and mite-attacked) were measured by a spectrophotometer (SolidSpec-3700, SHIMADZU) at the wavelength range from 300 to 1000 nm. The pigment contents of leaves in different health statuses (Fig. 2C) were calculated by leaf reflectance spectra (details in note S5 and fig. S46).

Supplementary Materials

The PDF file includes:

Notes S1 to S5
Figs. S1 to S47
Tables S1 to S6
Legends for movies S1 to S4
References

Other Supplementary Material for this manuscript includes the following:

Movies S1 to S4

REFERENCES AND NOTES

1. FAO, IFAD, UNICEF, WFP, WHO, "*The State of Food Security and Nutrition in the World 2023*" (2023); www.fao.org/documents/card/en/c/cc3017en.
2. D. Headey, M. Ruel, Food inflation and child undernutrition in low and middle income countries. *Nat. Commun.* **14**, 5761 (2023).
3. P. G. Kopelman, Obesity as a medical problem. *Nature* **404**, 635–643 (2000).
4. A. Fardet, Y. Boirie, Associations between food and beverage groups and major diet-related chronic diseases: An exhaustive review of pooled/meta-analyses and systematic reviews. *Nutr. Rev.* **72**, 741–762 (2014).
5. D. Bhowmik, K. S. Kumar, S. Paswan, S. Srivastava, Tomato-a natural medicine and its health benefits. *J. Pharmacogn. Phytochem.* **1**, 33–43 (2012).
6. FAO, *Agricultural production statistics 2000–2022* (FAOSTAT Analytical Briefs, no. 79, 2023); https://doi.org/10.4060/cc9205en.
7. S. Panno, S. Davino, A. G. Caruso, S. Bertacca, A. Crnogorac, A. Mandić, E. Noris, S. Matić, A review of the most common and economically important diseases that undermine the cultivation of tomato crop in the mediterranean basin. *Agronomy* **11**, 2188 (2021).
8. M. C. Picanço, L. Bacci, A. L. B. Crespo, M. M. M. Miranda, J. C. Martins, Effect of integrated pest management practices on tomato production and conservation of natural enemies. *Agri. For. Entomol.* **9**, 327–335 (2007).
9. M. Alsamir, T. Mahmood, R. Trethowan, N. Ahmad, An overview of heat stress in tomato (*Solanum lycopersicum* L.). *Saudi J. Biol. Sci.* **28**, 1654–1663 (2021).
10. R. Zhou, X. Yu, C.-O. Ottosen, E. Rosenqvist, L. Zhao, Y. Wang, W. Yu, T. Zhao, Z. Wu, Drought stress had a predominant effect over heat stress on three tomato cultivars subjected to combined stress. *BMC Plant Biol.* **17**, 24 (2017).
11. S. Fahad, O. Sönmez, S. Saud, D. Wang, C. Wu, M. Adnan, M. Arif, Amanullah, *Engineering Tolerance in Crop Plants Against Abiotic Stress* (CRC Press, ed. 1, 2021); www.taylorfrancis.com/books/9781003160717).
12. A. Migeon, F. Ferragut, L. A. Escudero-Colomar, K. Fiaboe, M. Knapp, G. J. De Moraes, E. Ueckermann, M. Navajas, Modelling the potential distribution of the invasive tomato red spider mite, Tetranychus evansi (Acari: Tetranychidae). *Exp. Appl. Acarol.* **48**, 199–212 (2009).
13. A. H. Molla, M. Manjurul Haque, M. Amdadul Haque, G. N. M. Ilias, Trichoderma-enriched biofertilizer enhances production and nutritional quality of tomato (*Lycopersicon esculentum* Mill.) and minimizes NPK fertilizer use. *Agric. Res.* **1**, 265–272 (2012).
14. W. W. Adams III, I. Terashima, The Leaf: A platform for performing photosynthesis, in *Advances in Photosynthesis and Respiration* (Springer International Publishing, 2018), vol. 44; http://link.springer.com/10.1007/978-3-319-93594-2.
15. Q. Liu, C. Zhang, H. Fang, L. Yi, M. Li, Indispensable biomolecules for plant defense against pathogens: NBS-LRR and "nitrogen pool" alkaloids. *Plant Sci.* **334**, 111752 (2023).
16. A. Künstler, G. Gullner, A. L. Ádám, J. K. Kolozsváriné Nagy, L. Király, The versatile roles of sulfur-containing biomolecules in plant defense—A road to disease resistance. *Plants* **9**, 1705 (2020).

17. H. Yin, Y. Cao, B. Marelli, X. Zeng, A. J. Mason, C. Cao, Soil sensors and plant wearables for smart and precision agriculture. *Adv. Mater.* **33**, 2007764 (2021).
18. A. V. Zubler, J.-Y. Yoon, Proximal methods for plant stress detection using optical sensors and machine learning. *Biosensors* **10**, 193 (2020).
19. G. Kitić, A. Tagarakis, N. Cselyuszka, M. Panić, S. Birgermajer, D. Sakulski, J. Matović, A new low-cost portable multispectral optical device for precise plant status assessment. *Comput. Electron. Agric.* **162**, 300–308 (2019).
20. D. Tholl, O. Hossain, A. Weinhold, U. S. R. Röse, Q. Wei, Trends and applications in plant volatile sampling and analysis. *Plant J.* **106**, 314–325 (2021).
21. Z. Tian, W. Ma, Q. Yang, F. Duan, Application status and challenges of machine vision in plant factory—A review. *Inf. Process Agric.* **9**, 195–211 (2022).
22. A. Lowe, N. Harrison, A. P. French, Hyperspectral image analysis techniques for the detection and classification of the early onset of plant disease and stress. *Plant Methods* **13**, 80 (2017).
23. H. J. Butler, M. R. McAinsh, S. Adams, F. L. Martin, Application of vibrational spectroscopy techniques to non-destructively monitor plant health and development. *Anal. Methods* **7**, 4059–4070 (2015).
24. S. Ghosal, D. Blystone, A. K. Singh, B. Ganapathysubramanian, A. Singh, S. Sarkar, An explainable deep machine vision framework for plant stress phenotyping. *Proc. Natl. Acad. Sci. U.S.A.* **115**, 4613–4618 (2018).
25. Y. Yan, M. Ni, F. Wang, Y. Yu, X. Gong, Y. Huang, W. Tao, C. Li, F. Wang, Metal–organic framework-based biosensor for detecting hydrogen peroxide in plants through color-to-thermal signal conversion. *ACS Nano* **16**, 15175–15187 (2022).
26. A. Singh, B. Ganapathysubramanian, A. K. Singh, S. Sarkar, Machine learning for high-throughput stress phenotyping in plants. *Trends Plant Sci.* **21**, 110–124 (2016).
27. J. J. Walsh, E. Mangina, S. Negrão, Advancements in imaging sensors and AI for plant stress detection: A systematic literature review. *Plant Phenomics* **6**, 0153 (2024).
28. S. A. D. M. Zahir, M. F. Jamlos, A. F. Omar, M. A. Jamlos, R. Mamat, J. Muncan, R. Tsenkova, Review–Plant nutritional status analysis employing the visible and near-infrared spectroscopy spectral sensor. *Spectrochim. Acta A. Mol. Biomol. Spectrosc.* **304**, 123273 (2024).
29. D. Son, J. Park, S. Lee, J. J. Kim, S. Chung, Integrating non-invasive VIS-NIR and bioimpedance spectroscopies for stress classification of sweet basil (*Ocimum basilicum* L.) with machine learning. *Biosens. Bioelectron.* **263**, 116579 (2024).
30. Y. Chai, C. Chen, X. Luo, S. Zhan, J. Kim, J. Luo, X. Wang, Z. Hu, Y. Ying, X. Liu, Cohabiting plant-wearable sensor in situ monitors water transport in plant. *Adv. Sci.* **8**, 2003642 (2021).
31. J. A. Barbosa, V. M. S. Freitas, L. H. B. Vidotto, G. R. Schleder, R. A. G. De Oliveira, J. F. Da Rocha, L. T. Kubota, L. C. S. Vieira, H. C. N. Tolentino, I. T. Neckel, A. L. Gobbi, M. Santhiago, R. S. Lima, Biocompatible wearable electrodes on leaves toward the on-site monitoring of water loss from plants. *ACS Appl. Mater. Interfaces* **14**, 22989–23001 (2022).
32. Z. Li, Y. Liu, O. Hossain, R. Paul, S. Yao, S. Wu, J. B. Ristaino, Y. Zhu, Q. Wei, Real-time monitoring of plant stresses via chemiresistive profiling of leaf volatiles by a wearable sensor. *Matter* **4**, 2553–2570 (2021).
33. G. Lee, O. Hossain, S. Jamalzadegan, Y. Liu, H. Wang, A. C. Saville, T. Shymanovich, R. Paul, D. Rotenberg, A. E. Whitfield, J. B. Ristaino, Y. Zhu, Q. Wei, Abaxial leaf surface-mounted multimodal wearable sensor for continuous plant physiology monitoring. *Sci. Adv.* **9**, eade2232 (2023).
34. K. Zhang, W. Li, H. Li, Y. Luo, Z. Li, X. Wang, X. Chen, A leaf-patchable reflectance meter for in situ continuous monitoring of chlorophyll content. *Adv. Sci.* **10**, 20232305552 (2023).
35. Y. Yang, T. He, P. Ravindran, F. Wen, P. Krishnamurthy, L. Wang, Z. Zhang, P. P. Kumar, E. Chae, C. Lee, All-organic transparent plant e-skin for noninvasive phenotyping. *Sci. Adv.* **10**, eadk7488 (2024).
36. C. Zhang, C. Zhang, X. Wu, J. Ping, Y. Ying, An integrated and robust plant pulse monitoring system based on biomimetic wearable sensor. *NPJ Flex. Electron.* **6**, 43 (2022).
37. J. J. Kim, L. K. Allison, T. L. Andrew, Vapor-printed polymer electrodes for long-term, on-demand health monitoring. *Sci. Adv.* **5**, eaaw0463 (2019).
38. J. J. Kim, R. Fan, L. K. Allison, T. L. Andrew, On-site identification of ozone damage in fruiting plants using vapor-deposited conducting polymer tattoos. *Sci. Adv.* **6**, eabc3296 (2020).
39. M. Jiang, S. Chen, P. Zhang, Y. Sun, J. Ye, Y. Deng, L. Li, J. Liu, Liquid metal enabled plant injectable electronics. *Mater. Today* **66**, 50–61 (2023).
40. E. Bihar, E. J. Strand, C. A. Crichton, M. N. Renny, I. Bonter, T. Tran, M. Atreya, A. Gestos, J. Haseloff, R. R. McLeod, G. L. Whiting, Self-healable stretchable printed electronic cryogels for in-vivo plant monitoring. *NPJ Flex Electron* **7**, 48 (2023).
41. Y. Lu, K. Xu, L. Zhang, M. Deguchi, H. Shishido, T. Arie, R. Pan, A. Hayashi, L. Shen, S. Akita, K. Takei, Multimodal plant healthcare flexible sensor system. *ACS Nano* **14**, 10966–10975 (2020).
42. J. A. Rogers, T. Someya, Y. Huang, Materials and mechanics for stretchable electronics. *Science* **327**, 1603–1607 (2010).
43. S. Xu, Y. Zhang, L. Jia, K. E. Mathewson, K.-I. Jang, J. Kim, H. Fu, X. Huang, P. Chava, R. Wang, S. Bhole, L. Wang, Y. J. Na, Y. Guan, M. Flavin, Z. Han, Y. Huang, J. A. Rogers, Soft microfluidic assemblies of sensors, circuits, and radios for the skin. *Science* **344**, 70–74 (2014).
44. J. K. Schjoerring, The molecular–physiological functions of mineral macronutrients and their consequences for deficiency symptoms in plants. *New Phytol.* **229**, 2446–2469 (2020).
45. G. A. Blackburn, Hyperspectral remote sensing of plant pigments. *J. Exp. Bot.* **58**, 855–867 (2006).
46. D. A. Sims, J. A. Gamon, Relationships between leaf pigment content and spectral reflectance across a wide range of species, leaf structures and developmental stages. *Remote Sens. Environ.* **81**, 337–354 (2002).
47. J. Zeng, W. Ping, A. Sanaeifar, X. Xu, W. Luo, J. Sha, Z. Huang, Y. Huang, X. Liu, B. Zhan, H. Zhang, X. Li, Quantitative visualization of photosynthetic pigments in tea leaves based on Raman spectroscopy and calibration model transfer. *Plant Methods* **17**, 4 (2021).
48. A. S. Parmagnani, G. Mannino, C. Brillada, M. Novero, L. Dall'Osto, M. E. Maffei, Biology of two-spotted spider mite (*Tetranychus urticae*): Ultrastructure, photosynthesis, guanine transcriptomics, carotenoids and chlorophylls metabolism, and decoyinine as a potential acaricide. *Int. J. Mol. Sci.* **24**, 1715 (2023).
49. F. C. Meinzer, Stomatal control of transpiration. *Trends Ecol. Evol.* **8**, 289–294 (1993).
50. M. Agarwal, S. Kr Gupta, K. K. Biswas, Development of efficient CNN model for Tomato crop disease identification. *Sustain. Comput. Inform. Syst.* **28**, 100407 (2020).
51. M. I. Hossain, S. Jahan, M. R. Al Asif, M. Samsuddoha, K. Ahmed, Detecting tomato leaf diseases by image processing through deep convolutional neural networks. *Smart Agr. Technol.* **5**, 100301 (2023).
52. S. Nandhini, K. Ashokkumar, Improved crossover based monarch butterfly optimization for tomato leaf disease classification using convolutional neural network. *Multimed. Tools Appl.* **80**, 18583–18610 (2021).
53. A. Fuentes, S. Yoon, D. S. Park, Deep learning-based phenotyping system with glocal description of plant anomalies and symptoms. *Front. Plant Sci.* **10**, 1321 (2019).
54. P. Baser, J. R. Saini, K. Kotecha, TomConv: An improved CNN model for diagnosis of diseases in tomato plant leaves. *Procedia Comput. Sci.* **218**, 1825–1833 (2023).
55. A. Abbas, Tomato plant disease detection using transfer learning with C-GAN synthetic images. *Comput. Electron. Agric.* **187**, 106279 (2021).
56. Y. Cen, Y. Huang, S. Hu, L. Zhang, J. Zhang, Early detection of bacterial wilt in tomato with portable hyperspectral spectrometer. *Remote Sens.* **14**, 2882 (2022).
57. M. Reis Pereira, F. N. D. Santos, F. Tavares, M. Cunha, Enhancing host-pathogen phenotyping dynamics: Early detection of tomato bacterial diseases using hyperspectral point measurement and predictive modeling. *Front. Plant Sci.* **14**, 1242201 (2023).
58. Y. Zhou, J. Chen, J. Ma, X. Han, B. Chen, G. Li, Z. Xiong, F. Huang, Early warning and diagnostic visualization of Sclerotinia infected tomato based on hyperspectral imaging. *Sci. Rep.* **12**, 21140 (2022).
59. M. Tomaszewski, J. Nalepa, E. Moliszewska, B. Ruszczak, K. Smykała, Early detection of *Solanum lycopersicum* diseases from temporally-aggregated hyperspectral measurements using machine learning. *Sci. Rep.* **13**, 7671 (2023).
60. S. Cui, E. A. A. Inocente, N. Acosta, H. M. Keener, H. Zhu, P. P. Ling, Development of fast E-nose system for early-stage diagnosis of aphid-stressed tomato plants. *Sensors* **19**, 3480 (2019).
61. S. Cui, L. Cao, N. Acosta, H. Zhu, P. P. Ling, Development of portable E-nose system for fast diagnosis of whitefly infestation in tomato plant in greenhouse. *Chemosensors* **9**, 297 (2021).
62. Z. Li, R. Paul, T. Ba Tis, A. C. Saville, J. C. Hansel, T. Yu, J. B. Ristaino, Q. Wei, Non-invasive plant disease diagnostics enabled by smartphone-based fingerprinting of leaf volatiles. *Nat. Plants* **5**, 856–866 (2019).
63. H. Chen, Z. You, X. Wang, Q. Qiu, Y. Ying, Y. Wang, An artificial olfactory sensor based on flexible metal–organic frameworks for sensing VOCs. *Chem. Eng. J* **446**, 137098 (2022).
64. H. Singh, P. Kumar, S. Chaudhari, M. Edelstein, Tomato grafting: A global perspective. *Horts* **52**, 1328–1336 (2017).
65. J. D. H. Keatinge, L.-J. Lin, A. W. Ebert, W. Y. Chen, J. d'A. Hughes, G. C. Luther, J.-F. Wang, M. Ravishankar, Overcoming biotic and abiotic stresses in the *Solanaceae* through grafting: Current status and future perspectives. *Biol. Agric. Hortic.* **30**, 272–287 (2014).
66. E. Sánchez-Rodríguez, R. Leyva, C. Constán-Aguilar, L. Romero, J. M. Ruiz, Grafting under water stress in tomato cherry: Improving the fruit yield and quality. *Ann. Appl. Biol.* **161**, 302–312 (2012).
67. M. Kawaguchi, A. Taji, D. Backhouse, M. Oda, Anatomy and physiology of graft incompatibility in solanaceous plants. *J. Hortic. Sci. Biotech.* **83**, 581–588 (2008).
68. M. P. Wolf, G. B. Salieb-Beugelaar, P. Hunziker, PDMS with designer functionalities—Properties, modifications strategies, and applications. *Prog. Polym. Sci.* **83**, 97–134 (2018).
69. J. Jiang, S. Zhang, B. Wang, H. Ding, Z. Wu, Hydroprinted liquid-alloy-based morphing electronics for fast-growing/tender plants: From physiology monitoring to habit manipulation. *Small* **16**, 2003833 (2020).
70. R. Pearcey, H. Mooney, P. Rundel, *Plant Physiological Ecology: Field Methods and Instrumentation* (Springer Science & Business Media, 2012.
71. O. Sagi, L. Rokach, Ensemble learning: A survey. *WIREs Data Min. Knowl.* **8**, e1249 (2018).

72. S. H. Jeong, S. Zhang, K. Hjort, J. Hilborn, Z. Wu, PDMS-based elastomer tuned soft, stretchable, and sticky for epidermal electronics. *Adv. Mater.* **28**, 5830–5836 (2016).

Acknowledgments

Funding: This research was partially supported by the National Natural Science Foundation of China (52188102 to H.D.), the National Key Research and Development Program of China (2024YFB4707902 to Z.W.), the Cross-research Support Program of Huazhong University of Science and Technology (2024JCYJ036 to Z.W.), and the experiment resources provided by the Flexible Electronics Manufacturing Laboratory of Huazhong University of Science and Technology. **Author contributions:** Conceptualization: Q.J., X.Z., and Z.W. Investigation: Q.J., X.Z., T.Z., W.L., X.D., Q.L., X.W., and X.C. Methodology: Q.J., X.Z., T.Z., and X.D. Data curation: Q.J., X.Z., T.Z., and X.D. Validation: Q.J., X.Z., T.Z., and X.D. Formal analysis: Q.J., X.Z., T.Z., W.L., and X.C. Software: Q.J. and T.Z. Project administration: Q.J. and Z.W. Visualization: Q.J., X.Z., T.Z., X.D., and W.L. Resources: X.W., Q.L., J.Y., Z.Y., H.D., X.C., and Z.W. Supervision: H.D., X.C., and Z.W. Writing—original draft: Q.J., X.Z., T.Z., W.L., X.C., and Z.W. Writing—review & editing: Q.J., W.L., J.Y., Z.Y., H.D., X.C., and Z.W. **Competing interests:** The authors declare that they have no competing interests. **Data and materials availability:** All data needed to evaluate the conclusions in the paper are present in the paper and/or the Supplementary Materials. The photos of tomato leaves in different health statuses, the transmission spectral data of these leaves, and the ML algorithms are openly available on Zenodo (https://zenodo.org/doi/10.5281/zenodo.15192884).

Submitted 13 February 2025
Accepted 23 May 2025
Published 27 June 2025
10.1126/sciadv.adw7279